Author Manuscript

Author Manuscript

Author Manuscript

Author Manuscript

HHS Public Access

Author manuscript

J Am Chem Soc. Author manuscript; available in PMC 2021 April 29.

Published in final edited form as:

J Am Chem Soc. 2020 April 29; 142(17): 7783–7794. doi:10.1021/jacs.9b13813.

Biodegradable gold nanoclusters with improved excretion due to pH-triggered hydrophobic-to-hydrophilic transition

Elizabeth M. Higbee-Dempsey[1], **Ahmad Amirshaghaghi**[2], **Matthew J. Case**[3], **Mathilde Bouché**[4], **Johoon Kim**[4], **David P. Cormode**[4], **Andrew Tsourkas**[2]

[1]Biochemistry and Molecular Biophysics Graduate Group, Perelman School of Medicine, University of Pennsylvania, Philadelphia, PA 19104.

[2]Department of Bioengineering, University of Pennsylvania, Philadelphia, PA 19104.

[3]Department of Radiation Oncology, University of Pennsylvania, Philadelphia, PA 19104.

[4]Department of Radiology, University of Pennsylvania, Philadelphia, PA 19104.

Abstract

Gold is a highly useful nanomaterial for many clinical applications, but its poor biodegradability can impair long-term physiological clearance. Large gold nanoparticles (20–200 nm), such as those required for long blood circulation times and appreciable tumor localization, often exhibit little to no dissolution and excretion. This can be improved by incorporating small gold particles within a larger entity, but elimination may still be protracted due to incomplete dispersion of gold. The present study describes a novel gold nanoparticle formulation capable of environmentally-triggered decomposition. Ultrasmall gold nanoparticles are coated with thiolated dextran, and hydrophobic acetal groups are installed through direct covalent modification of the dextran. This hydrophobic exterior allows gold to be densely packed within ~150-nm polymeric micelles. Upon exposure to an acidic environment, the acetal groups are cleaved and the gold nanoparticles become highly water-soluble, leading to destabilization of the micelle. Within 24 hours, the ultrasmall water-soluble gold particles are released from the micelle and readily dispersed. Micelle degradation and gold nanoparticle dispersion was imaged in cultured macrophages, and micelle-treated mice displayed progressive physiological clearance of gold, with > 85% elimination from the liver over three months. These particles present a novel nanomaterial formulation and address a critical unresolved barrier for clinical translation of gold nanoparticles.

INTRODUCTION

Gold nanoparticles (AuNPs) are among the most extensively studied nanoformulations, in part due to their easily manipulatable morphology and surface chemistry as well as their

Corresponding Author: atsourk@seas.upenn.edu.

§**Present Addresses**: M.J.C. current affiliation is College of Medicine, Medical University of South Carolina, Charleston, SC 29425.

Supporting Information

The Supporting Information is available free of charge on the ACS Publications website.

Experimental procedures, additional electron microscopy images, additional control mouse data, energy-dispersive X-ray spectroscopy analysis, NMR spectra, and detailed histopathology analysis (PDF)

The authors declare no competing financial interests.

Author Manuscript Author Manuscript Author Manuscript Author Manuscript

potential to be used in a variety of clinical applications.[1–3] Gold has attracted tremendous interest as a therapeutic agent – particularly in oncology – for applications including radiation sensitization[4–6] and photothermal therapy.[7–9] It has also been explored in various biomedical imaging modalities, including computed tomography (CT),[10–12] photoacoustic imaging,[13,14] and surface-enhanced Raman scattering.[15] Additionally, gold has been complexed with a range of other pharmaceuticals and imaging agents, as a scaffold for targeted delivery and multimodal activity.[12,16–18]

The majority of AuNPs and other nanomedicines are designed to be injected into peripheral veins, and once they have entered the blood stream, many particles will ultimately be phagocytosed by resident macrophages within the liver and spleen.[19] A particle's ability to target specific biological compartments is dependent on their physiochemical properties. For example, particle shape and surface chemistry can influence interactions with serum proteins and with cell membranes;[20,21] factors such as charge, hydrophobicity, and certain molecular markers may promote rapid uptake by phagocytic cells, while neutral hydrophilic coatings such as poly(ethylene) glycol (PEG) tend to delay phagocytosis and therefore confer longer serum circulation times.[22–24] Particle size also greatly impacts serum half-life; AuNPs smaller than ~10 nm tend to undergo rapid renal elimination, while particles larger than ~200 nm show accelerated sequestration in the liver and spleen.[25–27] Prolonged serum circulation can have a number of desirable effects, including increased localization of particles into tumors. This phenomenon is known as the enhanced permeability and retention effect (EPR), whereby circulating nanoparticles can extravasate through leaky tumor vasculature and persist due to poor lymphatic drainage.[28,29] It is important to note that, while particle accumulation in tumors may increase when compared with small molecular compounds, the total dose fraction delivered to the tumor is typically no more than 1% of the injected dose;[30] still, the majority of FDA-approved nanomaterials for oncology have been designed based on this principle.

While AuNPs may show beneficial biodistribution, they can also exhibit impaired physiological clearance due to gold's poor biodegradability. Gold particles cannot be easily broken down, even within the lysosomal compartment's highly acidic and hydrolytic environment, though a few processes may contribute to the slow degradation of gold over time (e.g., etching by thiols[31–33] or hydroxyl radicals[34,35]). As a result, gold nanoparticles commonly persist in tissue for weeks to months.[36–38] For example, in a landmark study by Sadauskas et al[39] in which 40-nm AuNPs were administered intravenously to mice, it was found that only 9% of gold was eliminated from the liver over the course of six months. Similarly, preclinical studies of 150-nm gold nanoshells showed no detectable reduction in total gold mass within the body, even at more than one year post-injection.[36] The long-term persistence of gold nanoparticles represents a significant concern for clinical application and regulatory approval.[40,41]

In order to improve the clearance of AuNPs while maintaining favorable pharmacokinetics, one strategy is to package clusters of small AuNP cores within a larger biodegradable construct. Such nanomaterials may be fabricated at an overall size that preserves favorable biodistribution, but the use of small gold particles can accelerate degradation and excretion. This is because small hydrophilic AuNPs have the potential to be renally excreted[42–45] and

Author Manuscript Author Manuscript Author Manuscript Author Manuscript

retained particles may have improved dissolution and deterioration due to their high surface-to-volume ratio.[37,46] Several such AuNP clusters have been reported, using a variety of complexing materials (e.g., polyphosphazene,[47,48] polylysine and silica,[49] amphiphilic block copolymers containing poly(ethylene glycol) and polylactic acid[50,51] or polycaprolactone,[52] liposomes,[53,54] and oligonucleotides[55]). One particularly successful strategy is the use of pH-sensitive materials, which undergo structural and chemical transformations in response to variations in pH between biological compartments. Biodegradable pH-responsive gold nanoclusters have proven useful in a number of applications, including endosomal escape,[56,57] tumor aggregation,[58–60] and drug release.[61,62]

Recently, our group reported gold-loaded polymeric micelles consisting of 1.9-nm dodecanethiol-capped AuNPs encapsulated by poly(ethylene glycol)-*block*-poly(ε-caprolactone) (PEG-PCL), with tunable micelle diameters of 30–150 nm.[63,64] The use of hydrophobic AuNPs allowed facile particle synthesis through micelle self-assembly, and dense packing of substantial gold mass within the particle core. These particles showed excellent tumor accumulation, biocompatibility, CT contrast, and radiosensitization. The use of small AuNPs conferred significant improvements in bioelimination compared to large solid cores, with ~30% reduction in the liver from day 2 to day 7 post-injection. In later studies using 0.9-nm AuNPs, this was further improved to ~40% reduction in the first week, and up to 65% over three months.[65] It was suspected that the residual biopersistence of gold resulted from incomplete dispersion of the hydrophobic particles.

To that end, we have developed a novel gold nanomaterial that transitions from hydrophobic to hydrophilic under acidic conditions (Figure 1). In particular, ultrasmall gold nanoparticles are coated with the pH-sensitive polymer, acetalated dextran.[66] The resulting particles can be encapsulated within the hydrophobic core of an amphiphilic diblock copolymer, forming a tightly-packed polymeric micelle. Upon exposure to low pH environments (e.g., the cellular lysosomal compartment), the pendent acetal groups on the acetalated dextran undergo hydrolysis, leading to disruption of the micelle and an increase in AuNP hydrophilicity. These small, dispersed AuNPs have a greater capacity for degradation and excretion, allowing for faster and more extensive bioelimination.

RESULTS AND DISCUSSION

A goal of this study was to produce dextran-coated gold nanoparticles that were smaller than the cutoff for renal clearance (estimated at 5–10 nm), which necessitated the production of even smaller AuNP cores (~2 nm in diameter). To produce these AuNPs, a protocol was adapted from Jadzinsky et al[67] using *p*-mercaptobenzoic acid as the capping ligand; this reaction could be scaled to produce ~1.7-nm gold particles with low polydispersity at yields of several hundred milligrams (“*p*MBA-AuNPs”; Figure 2a). These AuNPs were subsequently coated with a low-molecular-weight dextran (5 kDa) with a single terminal thiol group (Figure 2b).

Thiolated dextran was prepared by reductive amination of the terminal glucose moiety, which possesses a single transient aldehyde, with 3,3’-dithiobis(propanoic dihydrazide). 3,3’-dithiobis(propanoic dihydrazide) contains two terminal hydrazide groups and an

Author Manuscript Author Manuscript Author Manuscript Author Manuscript

internal disulfide. Hydrazide was chosen as the aldehyde linking group, as opposed to a primary amine, because it is generally resistant to acidic hydrolysis, especially when it is further stabilized by reduction with cyanoborohydride.[68,69] After conjugation of the dihydrazide with two dextran molecules, the disulfide was reduced with tris(2-carboxyethyl)phosphine (TCEP) to yield dextran-thiol, which was isolated by washing in 90% methanol. Notably, disulfides are generally capable of binding gold surfaces without prior reduction;[70,71] however, we found that the dextran disulfide dimer could not be efficiently conjugated with gold, presumably due to steric occlusion.

Hydrophilic *p*MBA-AuNPs were coated with dextran-thiol through simple ligand exchange by mixing the two reagents in aqueous solution (Figure 2c, 2e; Supporting Figure S1). This reaction contained a 10-fold molar excess of dextran-thiol relative to *p*-mercaptobenzoic acid, which could presumably facilitate substitution of these ligands on the AuNP surface. The successful addition of dextran and formation of "Dextran-AuNPs" was confirmed by analyzing the mass percentage of gold in purified particles: *p*MBA-coated AuNPs were approximately 80% gold, but this dropped to 31% gold after the ligand exchange reaction, due to the larger size of dextran (Table 1). Dextran-AuNPs were also examined by dynamic light scattering, and their average peak hydrodynamic diameter was 7.3 nm as calculated by intensity distribution (3.5 nm by number distribution).

Notably, these values are close to the reported size limits for renal filtration of negatively charged particles (~6–8 nm),[26,72] and it is possible that a fraction of Dextran-AuNPs may be unable to undergo renal filtration. However, much of the particle bulk derives from dextran, which is known to degrade within the lysosomal environment due to the activity of α-glucosidase and other enzymes, and it is conceivable that large Dextran-AuNPs could diminish in size over time due to hydrolysis of the dextran coating. In future experiments, it may also be possible to decrease the size of synthesized Dextran-AuNPs by using shorter dextran polymers (< 5 kDa) and/or smaller AuNP cores.

After conjugation of AuNPs with dextran, the hydroxyl groups on the dextran were covalently modified with pendant acetal groups (Figure 2d, 2e) to increase the hydrophobicity of the particles and enable their encapsulation within micelles. To append the acetal groups, Dextran-AuNPs were dissolved in dimethyl sulfoxide and then directly chemically reacted with 2-methoxypropene in the presence of the catalyst pyridinium-*p*-toluenesulfonate. The resulting particles, "AcetalDextran-AuNPs" (or "ADAs"), were no longer soluble in water; instead, they could be dissolved in organic solvents such as chloroform and toluene. This, along with an additional decrease in particle gold mass percentage (Table 1), was indicative of a distinct compositional change from Dextran-AuNPs and strongly suggests the successful application of acetal groups.

The behavior of ADAs was characterized under acidic conditions to evaluate their ability to transition back to hydrophilic Dextran-AuNPs. A range of aqueous buffers representing various physiological compartments were tested: PBS, pH 7.4, for blood; PBS, pH 6.8, for hypoxic tumors; and 0.3 M acetate buffer, pH 5.0, for lysosomes. First, hydrophobic ADAs were suspended in each of these buffers, which initially formed a turbid suspension due to the insolubility of these particles (Figure 3a, 3b). After several hours of mixing at 37 °C,

Author Manuscript Author Manuscript Author Manuscript Author Manuscript

particles at pH 7.4 and 6.8 appeared to remain unchanged. However, at pH 5.0, particles became fully water-soluble over the course of 12 hours, as evidenced by a dramatic increase in solution transmittance from cloudy (7.4 %T) to clear (60.7 %T). To further confirm this behavior, we suspended ADAs in serum at either pH 7.4 or pH 5.0 (Figure 3c). Initially, particles could be precipitated by centrifugation, which indicated insolubility due to their hydrophobic acetal coating. At later timepoints, particles at pH 5.0 lost this property and remained in solution even after high-speed centrifugation (16,000 × *g*, 10 min). This shift in solubility is consistent with the expected hydrolysis of the acetal groups at low pH.

Next, the ADAs were encapsulated within polymeric micelles. As noted, we have previously reported encapsulation of hydrophobic AuNPs using the biodegradable amphiphilic block copolymer PEG-PCL.[63,64] Following a similar approach, "AcetalDextran-AuNP-Micelles" ("ADAMs") were formed by simple mixing of PEG-PCL and gold particles in toluene, followed by emulsion in water and evaporation of toluene to drive micelle self-assembly (Figure 4a). Micelles were isolated by centrifugal sedimentation to yield 146-nm water-soluble particles, with a highly negative zeta potential of −31.5 ± 5.3 (Figure 4b). Particle structure and size were confirmed by transmission electron microscopy imaging (both standard- and Cryo-TEM) (Figure 4c). Micelles were observed to be stable in phosphate-buffered saline (PBS) at 4 °C for at least one week, as evidenced by consistent hydrodynamic diameter and EM structure (Figure 4d).

We then sought to determine whether ADAs could undergo a similar transition from hydrophobic to hydrophilic at pH 5.0 after being encapsulated in micelles. ADAMs were dissolved in serum at either pH 7.4 or pH 5.0 (Figure 3d). Although the micelles were fully soluble due to their outermost layer of PEG, their heavy gold cores meant they could be pelleted out of solution by high-speed centrifugation (16,000 × *g*, 10 min). When the micelles were mixed at 37 °C for 24 hours, those kept at pH 7.4 continued to display the same behavior, and could be pelleted. In contrast, those exposed to acidic conditions could no longer be sedimented at these centrifugation speeds. This suggests that the dispersed AuNPs no longer form a heavy gold core within the micelle and is consistent with our proposed model: the acidic environment leads to hydrolysis of the acetal groups, destabilization of the micelle core, and release of the Dextran-AuNPs. Importantly, the release of AuNPs from micelles may not require the complete degradation of the PEG-PCL, which is not expected to occur quickly under these conditions.[73]

To determine whether AuNPs can be released prior to complete micelle degradation, ADAMs were dissolved in buffers at either pH 7.4 or pH 5.0 and were examined by DLS (Figure 3e). Initially, particles displayed the expected size and structure within both environments, and particles incubated at pH 7.4 showed little alteration over time except for a small degree of aggregation. However, particles at pH 5.0 showed significant degradation after 24 hours of incubation at 37 °C, as indicated by the emergence of a subset of nanoparticles with a much smaller hydrodynamic diameter (average peak intensity, 33 nm). When these 24-hour samples were examined by TEM imaging (Figure 3f, 3g), we discovered several new structures, including 2-nm AuNPs that were either freely dispersed or present as small non-spherical clusters. No ADAMs were observed in these TEMs images; instead, large low-electron-density spheres appeared spatially distinct from small

Author Manuscript Author Manuscript Author Manuscript Author Manuscript

highly-electron-dense AuNPs. This suggests that empty PEG-PCL micelles are present in the sample, and may be the source of the large DLS peak found at this timepoint. The AuNP aggregates may presumably indicate partially de-acetalated Dextran-AuNPs; by this model, particles can leak out of micelles as they become increasingly hydrophilic, but retain partial hydrophobic regions that drive their self-assembly into small irregular clusters. Although further mechanistic analysis was not pursued in this study, these data strongly suggest that ADAMs can undergo structural degradation in a pH-depended manner.

We next examined the behavior of ADAMs in biological systems. Acetalated dextran has previously been proven to have toxicity comparable to that of poly(lactic-*co*-glycolic acid), an FDA-approved material; safety was confirmed in particle form and for the isolated breakdown products of acetal hydrolysis (i.e., acetone and methanol).[66] To confirm this behavior in the present formulation, ADAMs were incubated with an immortalized human liver cell line, HepG2, and a standard MTT assay was performed after 24 hours (Figure 5a). Cell viability of ~95% was seen up to at least 10 μg mL^{-1} gold, with no statistically significant decrease. Even at very high concentrations (80 μg mL^{-1} Au), viability was greater than 80% compared to media-only controls, suggesting good biocompatibility.

The biodegradation of ADAMS was also assessed in cell culture. As a control for these experiments, we prepared equivalent AuNP-loaded polymeric micelles that lacked pH sensitivity: 2-nm dodecanethiol-coated AuNPs ("C_{12}-AuNPs") formed into micelles using PEG-PCL ("C_{12}-AuNP-Micelles") (Supporting Figure S2).[63] Each micelle formulation was incubated with RAW 264.7 murine macrophages for 24 hours at 10 μg mL^{-1} gold; cells were then fixed, embedded, and sectioned for TEM analysis (Figure 5b,c). AuNPs could be clearly visualized within unstained cells and were localized to vesicular compartments. The pH-sensitive ADAMs showed considerable breakdown of the spherical micelle structure and dispersion of individual AuNPs. In contrast, control C_{12}-AuNP-Micelles retained a distinctly spherical shape; although some separated AuNPs could be observed, the clear unidirectional distribution pattern strongly suggested that this was an artefact of the TEM tissue-sectioning process. At this 24-hour timepoint, both micelle formulations had near equivalent accumulation of gold within (or associated with) cells (ADAMs: 10.7×10^{-9} μg per cell; C_{12}-AuNP-Micelles: 9.84×10^{-9} μg per cell).

Finally, the pharmacokinetics of ADAMs was evaluated. C57 black mice were injected intravenously with AcetalDextran-AuNP-Micelles at a dose of 100 mg Au per kg body weight, administered as a single bolus injection via the tail vein; this dose was selected based on similarity to other reported studies, as well as considerations such as sensitivity of gold detection in tissues.[57] To determine the circulation time of micelles in the bloodstream, blood samples were drawn at various timepoints post-injection and analyzed for gold content. Micelles displayed long circulation, with a half-life of 3.5 hours (Figure 6a).

A biodistribution analysis was performed by collecting organ samples at various timepoints for a total of twelve weeks and assessing tissue gold content using inductively-coupled plasma optical emission spectroscopy (ICP-OES) (Figure 6b). ADAMs displayed a tissue biodistribution pattern that is typical for nanoparticles of this size, with the majority of particles initially accumulating in the liver and spleen. However, we observed a substantial

Author Manuscript Author Manuscript Author Manuscript Author Manuscript

drop in gold levels in these organs over time. On average, liver gold decreased 86% over twelve weeks, while in the spleen it dropped 72% over that period. Liver clearance was also more rapid; levels began to decrease appreciably after the first week, while spleen levels remained high for the first four weeks. These clearance rates compare favorably to those reported in previous studies that used non-pH-sensitive gold micelles. When Poon et al[74] injected mice with 110-nm or 220-nm solid gold nanoparticles, they reported that ~40–50% of the total injected dose was present in the liver at 14 days post-injection, with approximately 2.5–8% found in the spleen; these values are higher than our approximate %ID of 8% in the liver and 4% in the spleen. In a study that was highly analogous to the present report, Al Zaki et al[65] described gold micelles containing 0.9-nm dodecanethiol-coated gold nanoparticles ("GPMs"). When comparing the two gold formulations and their long-term bioretention, ADAMs show a significantly lower %ID/g in the liver (%ID/g liver at 14 days, ADAMs ~9% vs GPMs ~30%; at 3 months, ADAMs ~3% vs GPMs ~15%). %ID/g in the spleen was more similar for the two formulations, but ADAMs displayed a greater decrease over time and a lower final level (%ID/g spleen at 14 days, ADAMs ~60% vs. GPMs ~50%; at 3 months, ADAMs ~16% vs GPMs ~20%). It is important to note that these cited studies contain several key differences in experimental methodology, and so a true comparison with the present work is not possible. Nevertheless, the results generally support our findings that pH-sensitive ADAMs represent an improvement in physiological clearance rates.

The mechanisms of micelle elimination were not examined in detail, but they likely involve endocytic uptake into cells, trafficking to lysosomes and other endosomal compartments, and exocytosis. In the liver, hepatocytes periodically exocytose their lysosomal contents into bile, where it is carried to the digestive tract and excreted in feces.[76–77] While we did not examine the gall bladder or intestines as part of this biodistribution analysis, we did collect feces and urine samples at specific timepoints throughout the experiment. We observed an appreciable amount of gold in the feces, particularly in samples which were collected at 1 day post-injection. Gold levels were lower in samples collected at later timepoints, indicating that the rate of fecal elimination slowed over time, but it is reasonable to assume the gold was excreted continuously over the elapsed time. This hepatobiliary excretion route may contribute to the faster elimination of gold from the liver vs. the spleen, where no equivalent system exists.

Sections of liver tissue were also examined by TEM imaging and energy-dispersive X-ray spectroscopy (EDX) (Supporting Figure S3, S4). Electron-dense 2-nm gold particles were observed within intracellular vesicles at 1 day post-injection. Furthermore, these particles were often well-dispersed, with partial or complete dissociation of the ADAM's spherical cluster structure. Similar images were acquired from mouse livers at 7 days post-injection, containing a spectrum of particle structures ranging from mostly-intact to fully-dissociated ADAMs (Supporting Figure S5). For the subset of micelles that showed little structural disruption, it is unknown whether this is due to more recent cellular uptake of ADAMs, variability in the particles' pH-responsive behavior, variations in the kinetics of their trafficking to acidic intracellular compartments, or other phenomena.

Author Manuscript Author Manuscript Author Manuscript Author Manuscript

Notably, by ICP-OES analysis, elemental gold could be detected in mouse urine at 24 hours post-injection (%ID/g tissue: 4.5 ± 0.5). This phenomenon was confirmed by examining urine samples via electron microscopy and EDX (Figure 6c; Supporting Figure S6). Gold was detected in the form of individual 2-nm AuNPs that were consistent in appearance to Dextran-AuNPs. These data suggest that intravenously injected AcetalDextran-AuNP-Micelles may be capable of breaking down into renally-excretable gold.

Throughout these studies, we examined mice for signs of drug-induced toxicity. Animals remained energetic and without visible signs of poor health (e.g. lethargy, noticeable changes in food intake, poor grooming, etc.). Injected animals displayed an initial transient drop in body weight (~10%); this weight loss was resolved by day 4, and generally increased throughout the twelve-week study (Figure 7a). Although mouse weight loss can arise from the stress-inducing effects of intravenous injection, repeated blood collection, and other handling procedures, we found that control saline-injected mice experienced a much smaller reduction in average body weight (~1%) despite similar manipulation (Supporting Figure S7). This indicates that the administration of ADAMs at the dose of 100 mg Au per kg body weight is likely responsible for this mild adverse event, and a lower dosage of ADAMs may be advisable for future studies.

Knowing the potential for high liver accumulation of particles, serum was collected from mice at 1, 3, and 7 days post-injection and analyzed for elevated liver enzymes: alanine transaminase (ALT), aspartate transaminase (AST), and alkaline phosphatase (ALP) (Figure 7b–d). These levels were widely recorded to be within normal limits, with the single exception of increased AST at 1 day. Notably, these assays involve colorimetric detection of enzymes;[78] at the 1 day timepoint, serum contained a substantial volume of gold particles that imparted a noticeable brown hue, which may have impacted analysis.

Finally, tissue samples were harvested from the kidney, liver, spleen, and lung at various timepoints post-injection (Figure 7e). Tissues were embedded with paraffin, stained with hematoxylin and eosin (H&E), and imaged by light microscopy. Slides were then independently evaluated by a board-certified veterinary pathologist (Supporting Information). Histological examination revealed no signs of acute or chronic pathology. Numerous cells were observed to contain pigmented foci, which were presumed to indicate regions of nanoparticle accumulation; these appeared in the liver (hepatic sinusoid and portal regions), spleen (red pulp), and kidney (interstitium), but not in the lung. These cells were not associated with any inflammation or parenchymal damage. Within the liver and spleen, these regions appeared immediately at Day 1 post-injection; in the kidney, no pigmented regions were found until 1 week post-injection. The early liver and spleen accumulation is perhaps made possible by the large sinusoidal slits and subsequent micelle phagocytosis by macrophages within these organs. Subsequently, the smaller 1.7 nm AuNP degradation products may be allowed to pass through glomerular fenestrations and accumulate within the kidney. The lack of observed accumulation altogether in the lung may be related to its lack of endothelial sinusoids and fenestrations that limit circulatory escape by both micelles and AuNPs. Notably, the number of pigmented cells within organs of accumulation decreased steadily over time.

Author Manuscript Author Manuscript Author Manuscript Author Manuscript

Altogether, these data suggest that ADAMs have low toxicity and that they can be cleared from the body over time. These findings imply that our gold nanoparticle formulation may be suitable for repeat administration, particularly compared to non-biodegradable gold particles; this is particularly important considering the ubiquity of multiple and metronomic dosage strategies in clinical cancer therapy.[79] In the current study, we elected to administer ADAMs via a single bolus dose in order to present a simplified pharmacokinetic analysis. However, we would propose that future studies examine the effects of repeat systemic administration, both on long-term clearance and on animal toxicity.[80–83]

CONCLUSION

Considering the extent of global research interest in gold nanoparticles and their therapeutic potential, it is important to address the lingering question of their physiological persistence. The reported strategy seeks to improve clearance while still maintaining favorable aspects of gold particle design. This has been achieved by utilizing a pH-sensitive polymer, acetalated dextran, which transitions from hydrophobic to hydrophilic in acidic conditions. Acetalated dextran containing a single terminal thiol group has been installed onto ultrasmall AuNPs using newly-described synthetic strategies. Clusters of these particles could then be encapsulated within polymeric micelles of favorable size, with high stability at pH 7.4. However, both the hydrophobic AuNPs and their larger polymeric assemblies showed rapid degradation in acidic buffers (pH 5.0) and in macrophage cell culture. Micelles were found to have good biocompatibility and serum pharmacokinetics; furthermore, they displayed progressive long-term clearance from accumulated tissues, including the liver and spleen. Collectively, these environmentally-responsive materials present an intriguing and effective strategy for the biodegradation of gold nanostructures.

Supplementary Material

Refer to Web version on PubMed Central for supplementary material.

ACKNOWLEDGMENT

The authors gratefully acknowledge Pratap Naha, Maryam Hajfathalian, and Clara Dong for support with ICP studies, and Jonathan Galarraga for support with NMR studies. The authors also thank David Chenoweth for advisement on dextran-thiol purification strategies, and Jessica F. Liu for her assistance in calculating blood half-life. This work was supported in part by the NIH/NCI R01CA181429 (A.T.), NIH/NIBIB R21EB023989 (A.T.), and the University Research Foundation Award (A.T.). This work was also carried out in part at the Singh Center for Nanotechnology, part of the National Nanotechnology Coordinated Infrastructure Program, which is supported by the National Science Foundation grant NNCI-1542153.

REFERENCES

(1). Yeh Y-C; Creran B; Rotello VM Gold Nanoparticles: Preparation, Properties, and Applications in Bionanotechnology. Nanoscale 2012, 4 (6), 1871–1880. [PubMed: 22076024]

(2). Jain S; Hirst DG; O'Sullivan JM Gold Nanoparticles as Novel Agents for Cancer Therapy. Br J Radiol 2012, 85 (1010), 101–113. [PubMed: 22010024]

(3). Elahi N; Kamali M; Baghersad MH Recent Biomedical Applications of Gold Nanoparticles: A Review. Talanta 2018, 184, 537–556. [PubMed: 29674080]

(4). Cooper DR; Bekah D; Nadeau JL Gold Nanoparticles and Their Alternatives for Radiation Therapy Enhancement. Front. Chem 2014, 2.

Author Manuscript Author Manuscript Author Manuscript Author Manuscript

(5). Haume K; Rosa S; Grellet S; Śmiałek MA; Butterworth KT; Solov'yov AV; Prise KM; Golding J; Mason NJ Gold Nanoparticles for Cancer Radiotherapy: A Review. Cancer Nanotechnol 2016, 7 (1).

(6). Laprise-Pelletier M; Simão T; Fortin M-A Gold Nanoparticles in Radiotherapy and Recent Progress in Nanobrachytherapy. Advanced Healthcare Materials 2018, 7 (16), 1701460.

(7). Abadeer NS; Murphy CJ Recent Progress in Cancer Thermal Therapy Using Gold Nanoparticles. J. Phys. Chem. C 2016, 120 (9), 4691–4716.

(8). Riley RS; Day ES Gold Nanoparticle-Mediated Photothermal Therapy: Applications and Opportunities for Multimodal Cancer Treatment. Wiley Interdisciplinary Reviews: Nanomedicine and Nanobiotechnology 2017, 9 (4), e1449.

(9). Vines JB; Yoon J-H; Ryu N-E; Lim D-J; Park H Gold Nanoparticles for Photothermal Cancer Therapy. Front. Chem 2019, 7.

(10). Xi D; Dong S; Meng X; Lu Q; Meng L; Ye J Gold Nanoparticles as Computerized Tomography (CT) Contrast Agents. RSC Adv. 2012, 2 (33), 12515–12524.

(11). Dreifuss T; Barnoy E; Motiei M; Popovtzer R Theranostic Gold Nanoparticles for CT Imaging In Design and Applications of Nanoparticles in Biomedical Imaging; Bulte JWM, Modo MMJ, Eds.; Springer International Publishing: Cham, 2017; pp 403–427.

(12). Mahan MM; Doiron AL Gold Nanoparticles as X-Ray, CT, and Multimodal Imaging Contrast Agents: Formulation, Targeting, and Methodology https://www.hindawi.com/journals/jnm/2018/5837276/ (accessed Aug 16, 2019).

(13). Li W; Chen X Gold Nanoparticles for Photoacoustic Imaging. Nanomedicine 2015, 10 (2), 299–320. 10.2217/nnm.14.169. [PubMed: 25600972]

(14). Fu Q; Zhu R; Song J; Yang H; Chen X Photoacoustic Imaging: Contrast Agents and Their Biomedical Applications. Advanced Materials 2019, 31 (6), 1805875.

(15). Li Y; Wei Q; Ma F; Li X; Liu F; Zhou M Surface-Enhanced Raman Nanoparticles for Tumor Theranostics Applications. Acta Pharmaceutica Sinica B 2018, 8 (3), 349–359. [PubMed: 29881674]

(16). Fratoddi I; Venditti I; Cametti C; Russo MV Gold Nanoparticles and Gold Nanoparticle-Conjugates for Delivery of Therapeutic Molecules. Progress and Challenges. J. Mater. Chem. B 2014, 2 (27), 4204–4220. [PubMed: 32261559]

(17). Chandran PR; Thomas RT Chapter 14 - Gold Nanoparticles in Cancer Drug Delivery In Nanotechnology Applications for Tissue Engineering; Thomas S, Grohens Y, Ninan N, Eds.; William Andrew Publishing: Oxford, 2015; pp 221–237.

(18). Kong F-Y; Zhang J-W; Li R-F; Wang Z-X; Wang W-J; Wang W Unique Roles of Gold Nanoparticles in Drug Delivery, Targeting and Imaging Applications. Molecules 2017, 22 (9).

(19). Feliu N; Docter D; Heine M; Pino P. del; Ashraf S; Kolosnjaj-Tabi J; Macchiarini P; Nielsen P; Alloyeau D; Gazeau F; Stauber RH; Parak WJ In Vivo Degeneration and the Fate of Inorganic Nanoparticles. Chem. Soc. Rev 2016, 45 (9), 2440–2457. [PubMed: 26862602]

(20). Qiu Y; Liu Y; Wang L; Xu L; Bai R; Ji Y; Wu X; Zhao Y; Li Y; Chen C Surface Chemistry and Aspect Ratio Mediated Cellular Uptake of Au Nanorods. Biomaterials 2010, 31 (30), 7606–7619. [PubMed: 20656344]

(21). Lazarovits J; Chen YY; Sykes EA; Chan WCW Nanoparticle–Blood Interactions: The Implications on Solid Tumour Targeting. Chem. Commun 2015, 51 (14), 2756–2767.

(22). Sahay G; Alakhova DY; Kabanov AV Endocytosis of Nanomedicines. Journal of Controlled Release 2010, 145 (3), 182–195. [PubMed: 20226220]

(23). Van Haute D; Berlin JM Challenges in Realizing Selectivity for Nanoparticle Biodistribution and Clearance: Lessons from Gold Nanoparticles. Ther Deliv 2017, 8 (9), 763–774. [PubMed: 28825391]

(24). Donahue ND; Acar H; Wilhelm S Concepts of Nanoparticle Cellular Uptake, Intracellular Trafficking, and Kinetics in Nanomedicine. Advanced Drug Delivery Reviews 2019.

(25). Albanese A; Tang PS; Chan WCW The Effect of Nanoparticle Size, Shape, and Surface Chemistry on Biological Systems. Annu. Rev. Biomed. Eng 2012, 14 (1), 1–16. [PubMed: 22524388]

Author Manuscript Author Manuscript Author Manuscript Author Manuscript

(26). Liu J; Yu M; Zhou C; Zheng J Renal Clearable Inorganic Nanoparticles: A New Frontier of Bionanotechnology. Materials Today 2013, 16 (12), 477–486.

(27). Hoshyar N; Gray S; Han H; Bao G The Effect of Nanoparticle Size on in Vivo Pharmacokinetics and Cellular Interaction. Nanomedicine 2016, 11 (6), 673–692. [PubMed: 27003448]

(28). Matsumura Y; Maeda H A New Concept for Macromolecular Therapeutics in Cancer Chemotherapy: Mechanism of Tumoritropic Accumulation of Proteins and the Antitumor Agent Smancs. Cancer Res. 1986, 46 (12 Pt 1), 6387–6392. [PubMed: 2946403]

(29). Jain RK; Stylianopoulos T Delivering Nanomedicine to Solid Tumors. Nature Reviews Clinical Oncology 2010, 7 (11), 653–664.

(30). Wilhelm S; Tavares AJ; Dai Q; Ohta S; Audet J; Dvorak HF; Chan WCW Analysis of Nanoparticle Delivery to Tumours. Nature Reviews Materials 2016, 1 (5), 16014.

(31). Schaaff TG; Whetten RL Controlled Etching of Au:SR Cluster Compounds. J. Phys. Chem. B 1999, 103 (44), 9394–9396.

(32). Wilcoxon JP; Provencio P Etching and Aging Effects in Nanosize Au Clusters Investigated Using High-Resolution Size-Exclusion Chromatography. J. Phys. Chem. B 2003, 107 (47), 12949–12957. 10.1021/jp027575y.

(33). Shichibu Y; Negishi Y; Tsunoyama H; Kanehara M; Teranishi T; Tsukuda T Extremely High Stability of Glutathionate-Protected Au25 Clusters Against Core Etching. Small 2007, 3 (5), 835–839. [PubMed: 17352431]

(34). Nowicka AM; Hasse U; Hermes M; Scholz F Hydroxyl Radicals Attack Metallic Gold. Angewandte Chemie International Edition 2010, 49 (6), 1061–1063. [PubMed: 20077451]

(35). Chen T-H; Nieh C-C; Shih Y-C; Ke C-Y; Tseng W-L Hydroxyl Radical-Induced Etching of Glutathione-Capped Gold Nanoparticles to Oligomeric Au I –Thiolate Complexes. RSC Advances 2015, 5 (56), 45158–45164.

(36). Gad SC; Sharp KL; Montgomery C; Payne JD; Goodrich GP Evaluation of the Toxicity of Intravenous Delivery of Auroshell Particles (Gold–Silica Nanoshells). Int J Toxicol 2012, 31 (6), 584–594. [PubMed: 23212452]

(37). Kolosnjaj-Tabi J; Javed Y; Lartigue L; Volatron J; Elgrabli D; Marangon I; Pugliese G; Caron B; Figuerola A; Luciani N; Pellegrino L; Alloyeau D; Gazeau F The One Year Fate of Iron Oxide Coated Gold Nanoparticles in Mice. ACS Nano 2015, 9 (8), 7925–7939. 10.1021/acsnano.5b00042. [PubMed: 26168364]

(38). Kolosnjaj-Tabi J; Volatron J; Gazeau F Basic Principles of In Vivo Distribution, Toxicity, and Degradation of Prospective Inorganic Nanoparticles for Imaging In Design and Applications of Nanoparticles in Biomedical Imaging; Bulte JWM, Modo MMJ, Eds.; Springer International Publishing: Cham, 2017; pp 9–41.

(39). Sadauskas E; Danscher G; Stoltenberg M; Vogel U; Larsen A; Wallin H Protracted Elimination of Gold Nanoparticles from Mouse Liver. Nanomedicine 2009, 5 (2), 162–169. [PubMed: 19217434]

(40). Havel HA Where Are the Nanodrugs? An Industry Perspective on Development of Drug Products Containing Nanomaterials. AAPS J 2016, 18 (6), 1351–1353. [PubMed: 27520380]

(41). Radomska A; Leszczyszyn J; Radomski MW The Nanopharmacology and Nanotoxicology of Nanomaterials: New Opportunities and Challenges. Adv Clin Exp Med 2016, 25 (1), 151–162. [PubMed: 26935510]

(42). Hainfeld JF; Slatkin DN; Focella TM; Smilowitz HM Gold Nanoparticles: A New X-Ray Contrast Agent. BJR 2006, 79 (939), 248–253. [PubMed: 16498039]

(43). Cho W-S; Cho M; Jeong J; Choi M; Han BS; Shin H-S; Hong J; Chung BH; Jeong J; Cho M-H Size-Dependent Tissue Kinetics of PEG-Coated Gold Nanoparticles. Toxicology and Applied Pharmacology 2010, 245 (1), 116–123. [PubMed: 20193702]

(44). Zhou C; Long M; Qin Y; Sun X; Zheng J Luminescent Gold Nanoparticles with Efficient Renal Clearance. Angewandte Chemie International Edition 2011, 50 (14), 3168–3172. [PubMed: 21374769]

(45). Naz F; Koul V; Srivastava A; Gupta YK; Dinda AK Biokinetics of Ultrafine Gold Nanoparticles (AuNPs) Relating to Redistribution and Urinary Excretion: A Long-Term in Vivo Study. Journal of Drug Targeting 2016, 24 (8), 720–729. [PubMed: 26837799]

Author Manuscript Author Manuscript Author Manuscript Author Manuscript

(46). Carlander U; Midander K; Hedberg YS; Johanson G; Bottai M; Karlsson HL Macrophage-Assisted Dissolution of Gold Nanoparticles. ACS Appl. Bio Mater. 2019, 2 (3), 1006–1016.

(47). Cheheltani R; Ezzibdeh RM; Chhour P; Pulaparthi K; Kim J; Jurcova M; Hsu JC; Blundell C; Litt HI; Ferrari VA; Allcock HR; Sehgal CM; Cormode DP Tunable, Biodegradable Gold Nanoparticles as Contrast Agents for Computed Tomography and Photoacoustic Imaging. Biomaterials 2016, 102, 87–97. [PubMed: 27322961]

(48). Bouché M; Pühringer M; Iturmendi A; Amirshaghaghi A; Tsourkas A; Teasdale I; Cormode DP Activatable Hybrid Polyphosphazene-AuNP Nanoprobe for ROS Detection by Bimodal PA/CT Imaging. ACS Appl. Mater. Interfaces 2019, 11 (32), 28648–28656. [PubMed: 31321973]

(49). Cassano D; Summa M; Pocoví-Martínez S; Mapanao A-K; Catelani T; Bertorelli R; Voliani V Biodegradable Ultrasmall-in-Nano Gold Architectures: Mid-Period In Vivo Distribution and Excretion Assessment. Particle & Particle Systems Characterization 2019, 36 (2), 1800464.

(50). Tam JM; Tam JO; Murthy A; Ingram DR; Ma LL; Travis K; Johnston KP; Sokolov KV Controlled Assembly of Biodegradable Plasmonic Nanoclusters for Near-Infrared Imaging and Therapeutic Applications. ACS Nano 2010, 4 (4), 2178–2184. [PubMed: 20373747]

(51). Tam JM; Murthy AK; Ingram DR; Nguyen R; Sokolov KV; Johnston KP Kinetic Assembly of Near-IR Active Gold Nanoclusters Using Weakly Adsorbing Polymers to Control Size. Langmuir 2010, 26 (11).

(52). Huang P; Lin J; Li W; Rong P; Wang Z; Wang S; Wang X; Sun X; Aronova M; Niu G; Leapman RD; Nie Z; Chen X Biodegradable Gold Nanovesicles with Ultra-Strong Plasmonic Coupling Effect for Photoacoustic Imaging and Photothermal Therapy. Angew Chem Int Ed Engl 2013, 52 (52), 13958–13964. [PubMed: 24318645]

(53). Troutman TS; Barton JK; Romanowski M Biodegradable Plasmon Resonant Nanoshells. Advanced Materials 2008, 20 (13), 2604–2608. [PubMed: 21494416]

(54). Rengan AK; Bukhari AB; Pradhan A; Malhotra R; Banerjee R; Srivastava R; De A In Vivo Analysis of Biodegradable Liposome Gold Nanoparticles as Efficient Agents for Photothermal Therapy of Cancer. Nano Lett. 2015, 15 (2), 842–848. [PubMed: 25554860]

(55). Chou LYT; Zagorovsky K; Chan WCW DNA Assembly of Nanoparticle Superstructures for Controlled Biological Delivery and Elimination. Nature Nanotechnology 2014, 9 (2), 148–155.

(56). Guo S; Huang Y; Jiang Q; Sun Y; Deng L; Liang Z; Du Q; Xing J; Zhao Y; Wang PC; Dong A; Liang X-J Enhanced Gene Delivery and SiRNA Silencing by Gold Nanoparticles Coated with Charge-Reversal Polyelectrolyte. ACS Nano 2010, 4 (9), 5505–5511. [PubMed: 20707386]

(57). Plaza-Ga I; Manzaneda-González V; Kisovec M; Almendro-Vedia V; Muñoz-Úbeda M; Anderluh G; Guerrero-Martínez A; Natale P; López Montero I PH-Triggered Endosomal Escape of Pore-Forming Listeriolysin O Toxin-Coated Gold Nanoparticles. J Nanobiotechnology 2019, 17 (1), 108. [PubMed: 31623647]

(58). Liu X; Chen Y; Li H; Huang N; Jin Q; Ren K; Ji J Enhanced Retention and Cellular Uptake of Nanoparticles in Tumors by Controlling Their Aggregation Behavior. ACS Nano 2013, 7 (7), 6244–6257. [PubMed: 23799860]

(59). Nam J; La W-G; Hwang S; Ha YS; Park N; Won N; Jung S; Bhang SH; Ma Y-J; Cho Y-M; Jin M; Han J; Shin J-Y; Wang EK; Kim SG; Cho S-H; Yoo J; Kim B-S; Kim S PH-Responsive Assembly of Gold Nanoparticles and “Spatiotemporally Concerted” Drug Release for Synergistic Cancer Therapy. ACS Nano 2013, 7 (4), 3388–3402. [PubMed: 23530622]

(60). Ansar SM; Chakraborty S; Kitchens CL PH-Responsive Mercaptoundecanoic Acid Functionalized Gold Nanoparticles and Applications in Catalysis. Nanomaterials (Basel) 2018, 8 (5).

(61). Xia F; Hou W; Zhang C; Zhi X; Cheng J; de la Fuente JM; Song J; Cui D PH-Responsive Gold Nanoclusters-Based Nanoprobes for Lung Cancer Targeted near-Infrared Fluorescence Imaging and Chemo-Photodynamic Therapy. Acta Biomater 2018, 68, 308–319. [PubMed: 29292171]

(62). Kazmi SAR; Qureshi MZ; Ali S; Masson J-F In Vitro Drug Release and Biocatalysis from PH-Responsive Gold Nanoparticles Synthesized Using Doxycycline. Langmuir 2019, 35 (49), 16266–16274. [PubMed: 31710229]

Author Manuscript Author Manuscript Author Manuscript Author Manuscript

(63). Al Zaki A; Joh D; Cheng Z; De Barros ALB; Kao G; Dorsey J; Tsourkas A Gold-Loaded Polymeric Micelles for Computed Tomography-Guided Radiation Therapy Treatment and Radiosensitization. ACS Nano 2014, 8 (1), 104–112. [PubMed: 24377302]

(64). McQuade C; Zaki AA; Desai Y; Vido M; Sakhuja T; Cheng Z; Hickey RJ; Joh D; Park S-J; Kao G; Dorsey JF; Tsourkas A A Multifunctional Nanoplatform for Imaging, Radiotherapy, and the Prediction of Therapeutic Response. Small 2015, 11 (7), 834–843. [PubMed: 25264301]

(65). Zaki AA; Hui JZ; Higbee E; Tsourkas A Biodistribution, Clearance, and Toxicology of Polymeric Micelles Loaded with 0.9 or 5 Nm Gold Nanoparticles. J Biomed Nanotechnol 2015, 11 (10), 1836–1846. [PubMed: 26502646]

(66). Bachelder EM; Beaudette TT; Broaders KE; Dashe J; Fréchet JMJ Acetal-Derivatized Dextran: An Acid-Responsive Biodegradable Material for Therapeutic Applications. J. Am. Chem. Soc 2008, 130 (32), 10494–10495. [PubMed: 18630909]

(67). Jadzinsky PD; Calero G; Ackerson CJ; Bushnell DA; Kornberg RD Structure of a Thiol Monolayer-Protected Gold Nanoparticle at 1.1 Å Resolution. Science 2007, 318 (5849), 430–433. [PubMed: 17947577]

(68). O'Donnell JP The Reaction of Amines with Carbonyls: Its Significance in the Nonenzymatic Metabolism of Xenobiotics. Drug Metabolism Reviews 1982, 13 (1), 123–59. [PubMed: 6806054]

(69). Hermanson G Bioconjugate Techniques, 1st ed; Elsevier, 1996.

(70). Grönbeck H; Curioni A; Andreoni W Thiols and Disulfides on the Au(111) Surface: The Headgroup–Gold Interaction. J. Am. Chem. Soc 2000, 122 (16), 3839–3842.

(71). Love JC; Estroff LA; Kriebel JK; Nuzzo RG; Whitesides GM Self-Assembled Monolayers of Thiolates on Metals as a Form of Nanotechnology. Chem. Rev 2005, 105 (4), 1103–1170. [PubMed: 15826011]

(72). Longmire M; Choyke PL; Kobayashi H Clearance Properties of Nano-Sized Particles and Molecules as Imaging Agents: Considerations and Caveats. Nanomedicine (Lond) 2008, 3 (5), 703–717. [PubMed: 18817471]

(73). Hernández AR; Contreras OC; Acevedo JC; Moreno LGN Poly(ε-Caprolactone) Degradation Under Acidic and Alkaline Conditions. American Journal of Polymer Science 2013, 3 (4), 70–75.

(74). Poon W; Zhang Y-N; Ouyang B; Kingston BR; Wu JLY; Wilhelm S; Chan WCW Elimination Pathways of Nanoparticles. ACS Nano 2019, 13 (5), 5785–5798. [PubMed: 30990673]

(75). Renaud G; Hamilton RL; Havel RJ Hepatic Metabolism of Colloidal Gold-Low-Density Lipoprotein Complexes in the Rat: Evidence for Bulk Excretion of Lysosomal Contents into Bile. Hepatology 1989, 9 (3), 380–392. [PubMed: 2920994]

(76). Zhang Y-N; Poon W; Tavares AJ; McGilvray ID; Chan WCW Nanoparticle–Liver Interactions: Cellular Uptake and Hepatobiliary Elimination. Journal of Controlled Release 2016, 240, 332–348. [PubMed: 26774224]

(77). Wang H; Thorling CA; Liang X; Bridle KR; Grice JE; Zhu Y; Crawford DHG; Xu ZP; Liu X; Roberts MS Diagnostic Imaging and Therapeutic Application of Nanoparticles Targeting the Liver. J. Mater. Chem. B 2015, 3 (6), 939–958. [PubMed: 32261972]

(78). Huang X-J; Choi Y-K; Im H-S; Yarimaga O; Yoon E; Kim H-S Aspartate Aminotransferase (AST/GOT) and Alanine Aminotransferase (ALT/GPT) Detection Techniques. Sensors (Basel) 2006, 6 (7), 756–782.

(79). Aston WJ; Hope DE; Nowak AK; Robinson BW; Lake RA; Lesterhuis WJ A Systematic Investigation of the Maximum Tolerated Dose of Cytotoxic Chemotherapy with and without Supportive Care in Mice. BMC Cancer 2017, 17 (1), 684(1) [PubMed: 29037232]

(80). Lasagna-Reeves C; Gonzalez-Romero D; Barria MA; Olmedo I; Clos A; Sadagopa Ramanujam VM; Urayama A; Vergara L; Kogan MJ; Soto C Bioaccumulation and Toxicity of Gold Nanoparticles after Repeated Administration in Mice. Biochemical and Biophysical Research Communications 2010, 393 (4), 649–655. [PubMed: 20153731]

(81). Rambanapasi C; Zeevaart JR; Buntting H; Bester C; Kotze D; Hayeshi R; Grobler A Bioaccumulation and Subchronic Toxicity of 14 Nm Gold Nanoparticles in Rats. Molecules 2016, 21 (6).

Author Manuscript Author Manuscript Author Manuscript Author Manuscript

(82). Weaver JL; Tobin GA; Ingle T; Bancos S; Stevens D; Rouse R; Howard KE; Goodwin D; Knapton A; Li X; Shea K; Stewart S; Xu L; Goering PL; Zhang Q; Howard PC; Collins J; Khan S; Sung K; Tyner KM Evaluating the Potential of Gold, Silver, and Silica Nanoparticles to Saturate Mononuclear Phagocytic System Tissues under Repeat Dosing Conditions. Part Fibre Toxicol 2017, 14 (1), 25. [PubMed: 28716104]

(83). Yang L; Kuang H; Zhang W; Aguilar ZP; Wei H; Xu H Comparisons of the Biodistribution and Toxicological Examinations after Repeated Intravenous Administration of Silver and Gold Nanoparticles in Mice. Scientific Reports 2017, 7 (1), 1–12. [PubMed: 28127051]

Author Manuscript Author Manuscript Author Manuscript Author Manuscript

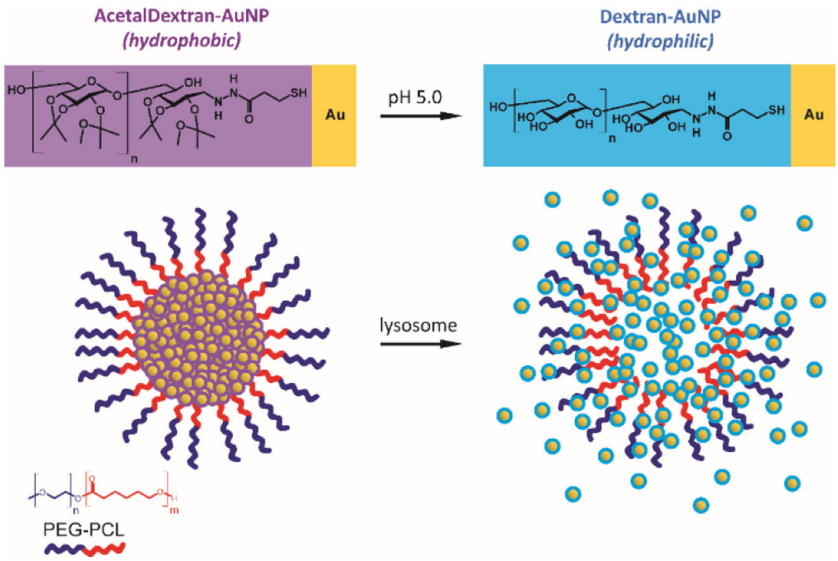

Figure 1.

Schematic showing the dispersion of AcetalDextran-AuNPs from micelles when placed in an acidic environment. Ultrasmall gold particles are coated with a hydrophobic pH-sensitive polymer, acetalated dextran; upon exposure to low pH environments, this hydrophobic coating becomes hydrophilic. Polymeric micelles encapsulating these materials will be stable at standard physiological pH but will dissociate within the lysosome, allowing dispersion of soluble AuNPs.

Author Manuscript
Author Manuscript
Author Manuscript
Author Manuscript

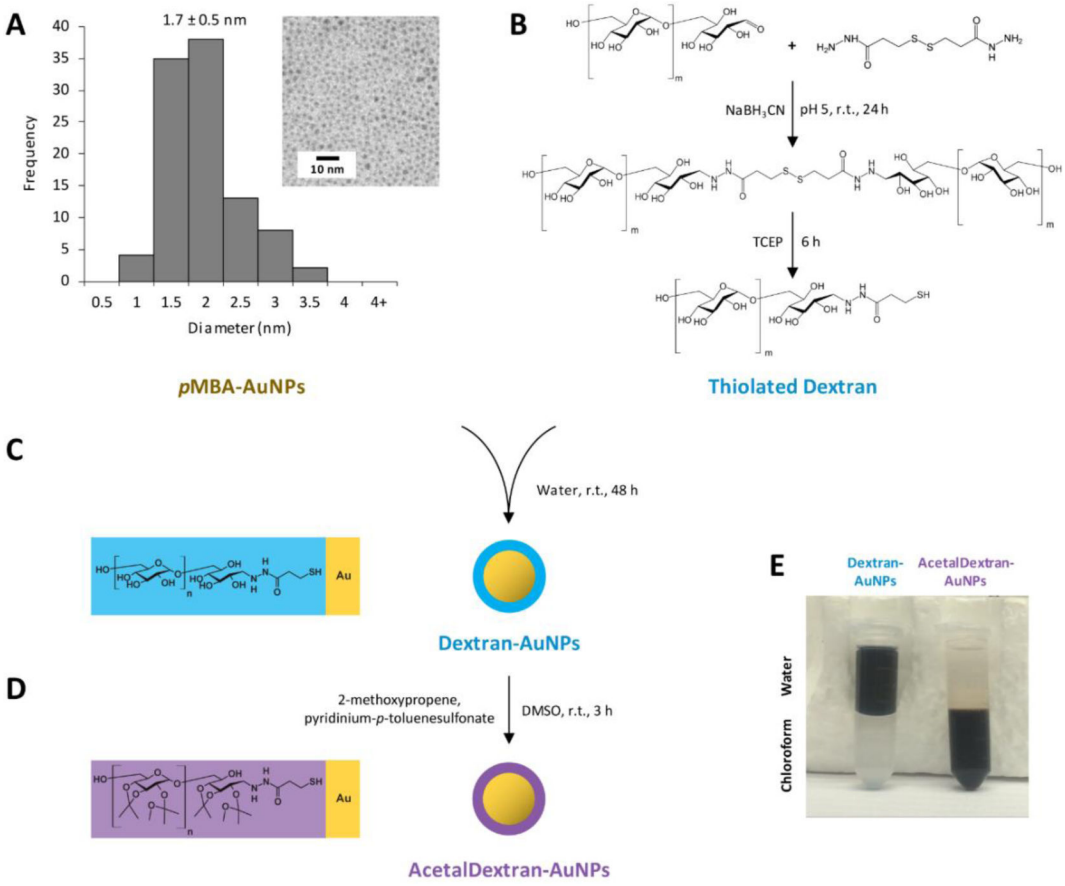

Figure 2.

Synthesis of AcetalDextran-AuNPs. (a) Ultrasmall hydrophilic gold nanoparticles (AuNPs) were synthesized using *p*-mercaptobenzoic acid (*p*MBA) as a capping ligand; particles had a mean core diameter of 1.7 ± 0.5 nm (SEM). Inset shows TEM image of dried particles. (b) Dextran (5 kDa) was combined with 3,3'-dithiobis(propanoic dihydrazide) to install a terminal thiol group. (c) *p*MBA-AuNPs were coated with thiolated dextran via ligand exchange, yielding Dextran-AuNPs. (d) Dextran-AuNPs were covalently modified with acetal groups, yielding AcetalDextran-AuNPs. (e) Demonstration of water-soluble Dextran-AuNPs vs. chloroform-soluble AcetalDextran-AuNPs.

Author Manuscript Author Manuscript Author Manuscript Author Manuscript

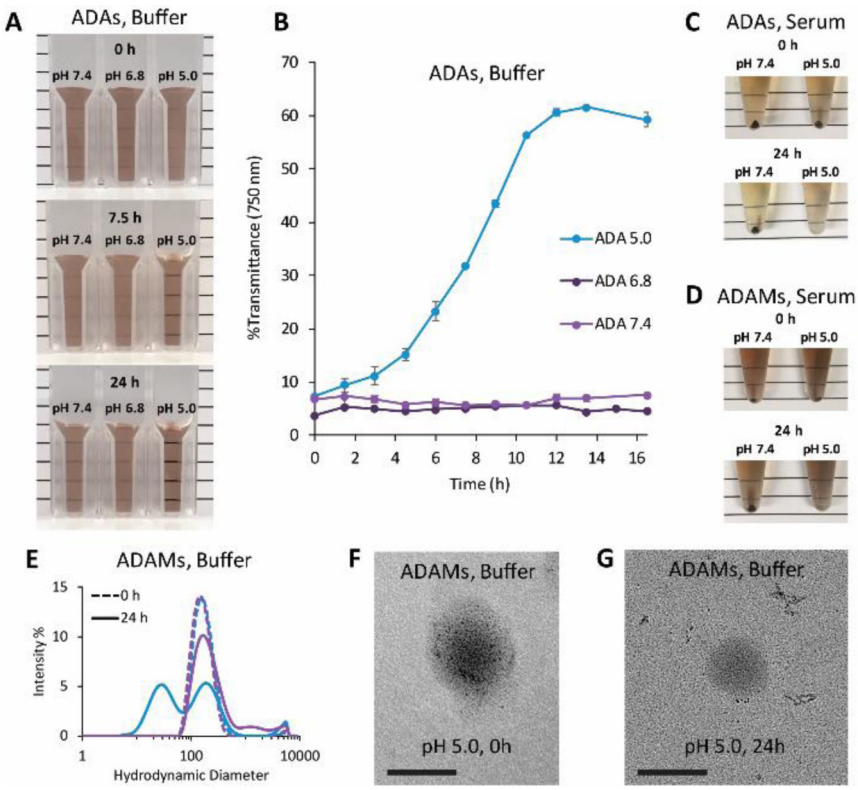

Figure 3.

pH-dependent solubility of particles incubated at pH 7.4 (PBS), pH 6.8 (PBS), or pH 5.0 (0.3 M acetate). (a) AcetalDextran-AuNPs (ADAs) were suspended in buffers (1.5 mg mL^{-1} by dry particle weight) and incubated at 37 °C under constant agitation for a total of 24 hours. Representative images shown. (b) Aliquots of ADAs were removed and measured for absorbance at 750 nm; results expressed as percent transmittance, average of three measurements ± standard deviation. (c,d) ADAs or AcetalDextran-AuNP-Micelles (ADAMs) were suspended in serum (0.04 mg mL^{-1} by Au, 1 mL) and incubated at 37 °C under constant agitation for a total of 24 hours. Particles were centrifuged at 16,000 × *g* for 10 minutes; separate tubes were prepared for each timepoint. (e) ADAMs were suspended in buffers (pH 7.4, purple lines; pH 5.0, blue lines) and hydrodynamic diameters were determined by dynamic light scattering. (f,g) Electron microscopy images of ADAMs suspended in buffer at pH 5.0 for either several seconds or 24 hours. Particles were diluted in water to reduce salt concentration and then dried on a grid for imaging. Scale bar = 100 nm.

Author Manuscript Author Manuscript Author Manuscript Author Manuscript

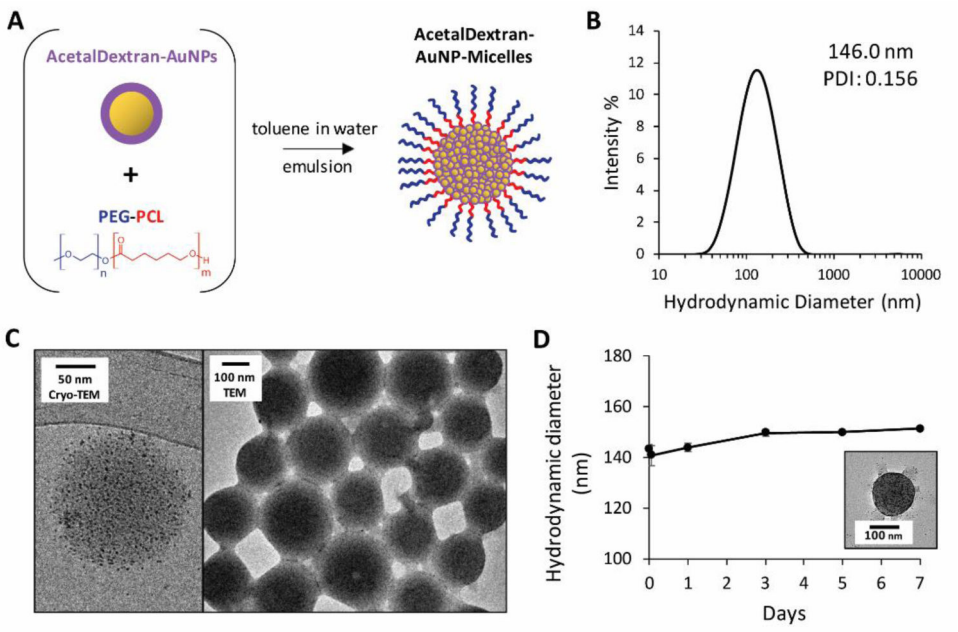

Figure 4.

Formation and characterization of AcetalDextran-AuNP-Micelles. (a) AcetalDextran-AuNPs and PEG-PCL were dissolved in toluene and then suspended in water to form an emulsion, driving self-assembly of AcetalDextran-AuNP-Micelles. (b) Hydrodynamic diameter of micelles determined via dynamic light scattering. The average peak hydrodynamic diameter was 146 nm. (c) Electron microscopy imaging of micelles in water via Cryo-TEM and standard TEM. (d) Hydrodynamic diameter of micelles in PBS at 4 °C, recorded immediately after suspension and at 1 hour, 1 day, 3 days, 5 days, and 7 days (average of three measurements, ± SEM). At 7 days, the sample was diluted 10-fold in water to reduce salt concentration and then imaged by TEM (inset).

Author Manuscript Author Manuscript Author Manuscript Author Manuscript

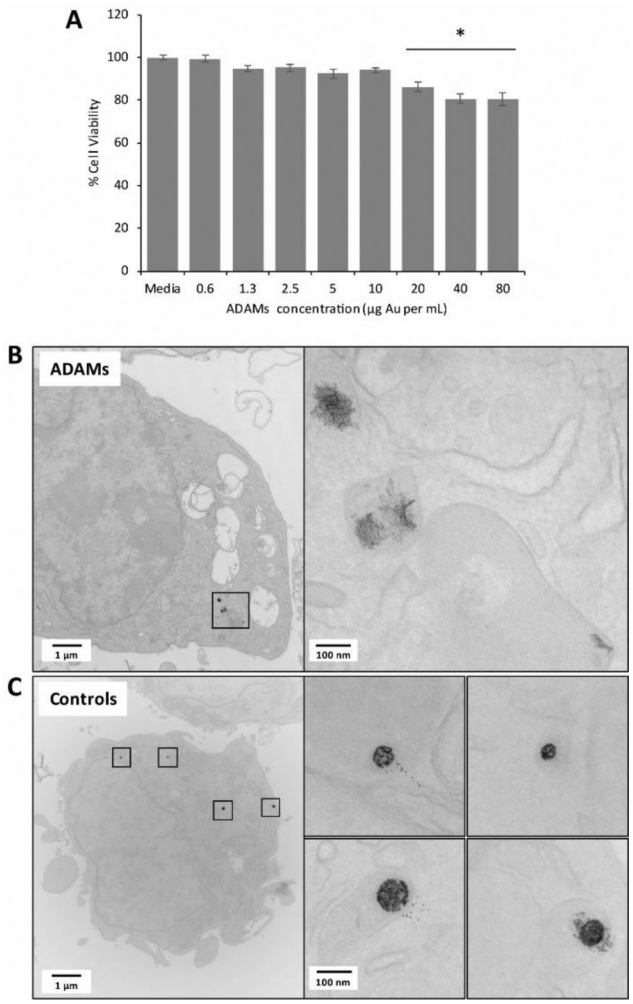

Figure 5.

AcetalDextran-AuNP-Micelles (ADAMs) in cell culture. (a) ADAMs were incubated with HepG2 human liver cells at various concentrations (expressed as μg Au per mL of cell culture solution) for 24 hours, and cytotoxicity was assessed by MTT assay. % Cell viability was calculated in relation to media-only controls; statistical comparison was performed using one-way ANOVA with post-hoc Tukey HSD test; $*p < 0.05$ relative to media controls. (b,c) ADAMs or control micelles (C_{12}-AuNP-Micelles) were incubated with RAW 264.7 murine macrophages at 10 μg mL^{-1}Au for 24 hours. Cells were fixed and imaged by electron microscopy. Single cell shown for each condition, with expanded images on left.

Author Manuscript Author Manuscript Author Manuscript Author Manuscript

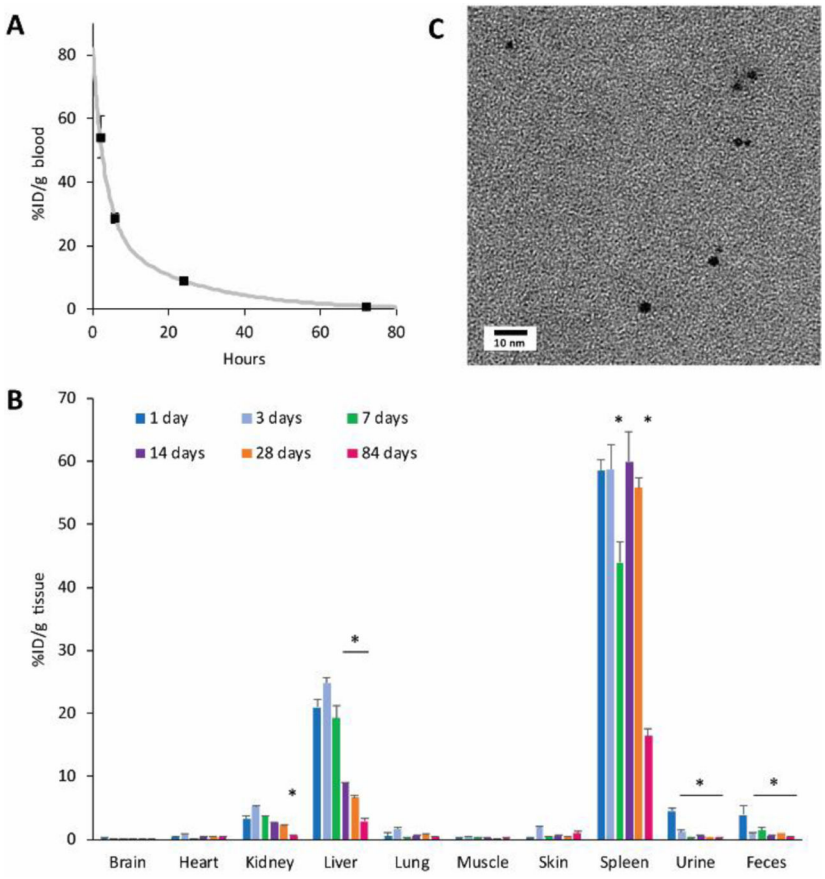

Figure 6.

In vivo pharmacokinetics and biodistribution of ADAMs. Mice were injected intravenously with 100 mg Au per kg body weight, and samples were collected at various timepoints post-injection ($n = 3$ mice per timepoint, expressed as average ± SEM). (a) Blood samples were analyzed by ICP-OES to determine gold content; curve-fitting was performed using MATLAB software. (b) Tissue and fluid samples were analyzed by ICP-OES to determine gold content ($n = 3$ mice per timepoint, expressed as average ± SEM.) Note that feces and urine values represent samples collected on the day of sacrifice, and do not represent the cumulative excretions between timepoints. Statistical comparison was performed using one-way ANOVA with post-hoc Tukey HSD test; $*p < 0.05$ relative to measurement at 1 day. (c) Urine was collected at 24 hours post-injection, diluted 1:1 in pure water, and imaged by electron microscopy. Electron-dense 2-nm particles are consistent with the appearance of Dextran-AuNPs.

Author Manuscript Author Manuscript Author Manuscript Author Manuscript

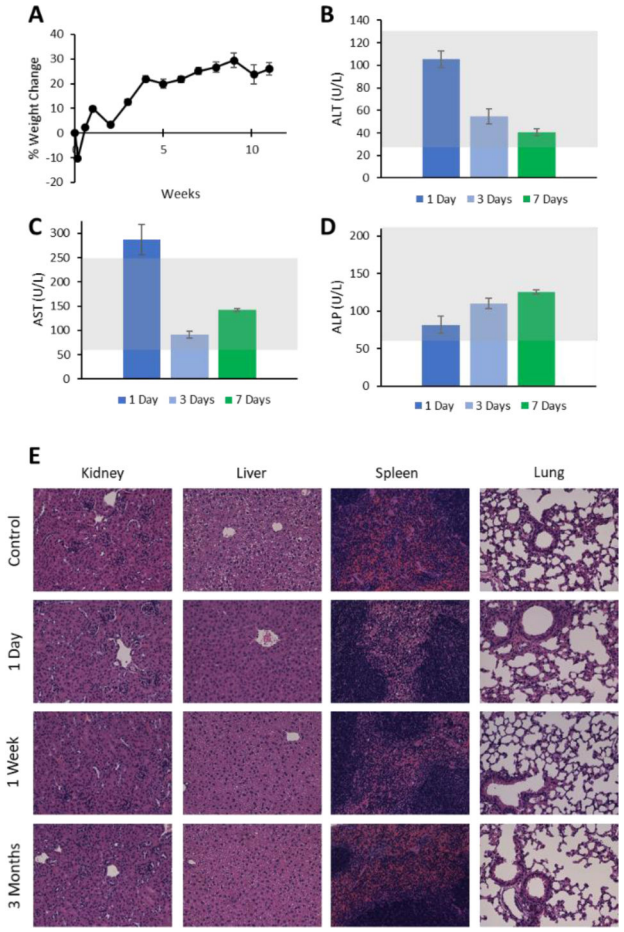

Figure 7.

Safety profile of AcetalDextran-AuNP-Micelles after injection of 100 mg Au per kg body weight. (a) Percent change in mouse body weight over time, normalized to pre-injection weight. (b-d) Serum measurements of alanine aminotransferase, aspartate aminotransferase, and alkaline phosphatase at various times post-injection. Gray shading represents standard clinical range for healthy mice. $n = 3$ mice per group, ± standard error of the mean. (e) Representative histological images of mouse organ tissues at various timepoints post-injection. Tissues were paraffin-embedded and stained with H&E.

Author Manuscript

Author Manuscript

Author Manuscript

Author Manuscript

Table 1.

Physiochemical parameters for AcetalDextran-AuNP-Micelles and precursor gold nanoparticles.

	% Au [w/w][a]	Core diameter[b]	Hydrodynamic diameter[c]	Solubility[d]	pH sensitivity[e]
*p*MBA-AuNPs	79.3%	1.7 ± 0.5 nm	5.0 nm PDI: 0.251	Water	No
Dextran-AuNPs	31.0%	2.1 ± 0.5 nm	7.3 nm PDI: 0.246	Water, DMSO	No
AcetalDextran-AuNPs	13.8%	2.1 ± 0.6 nm	n/a	Acetone, Toluene, Chloroform	Yes
AcetalDextran-AuNP-Micelles	11.4%	111.1 ± 38 nm	146.0 nm PDI: 0.156	Water	Yes

[a] Percent gold mass measured by ICP-OES.

[b] Core diameters measured by transmission electron microscopy, expressed as the average of 40–100 particle measurements, ± standard deviation.

[c] Hydrodynamic diameters measured by dynamic light scattering, expressed as the mean intensity and polydispersity index averaged for three measurements (*p*MBA-AuNPs and Dextran-AuNPs, one batch; AcetalDextran-AuNP-Micelles, six batches).

[d] Solubility is not comprehensive.

[e] pH sensitivity refers to observed changes in particle solubility and sedimentation behavior after incubation at pH 5.0.